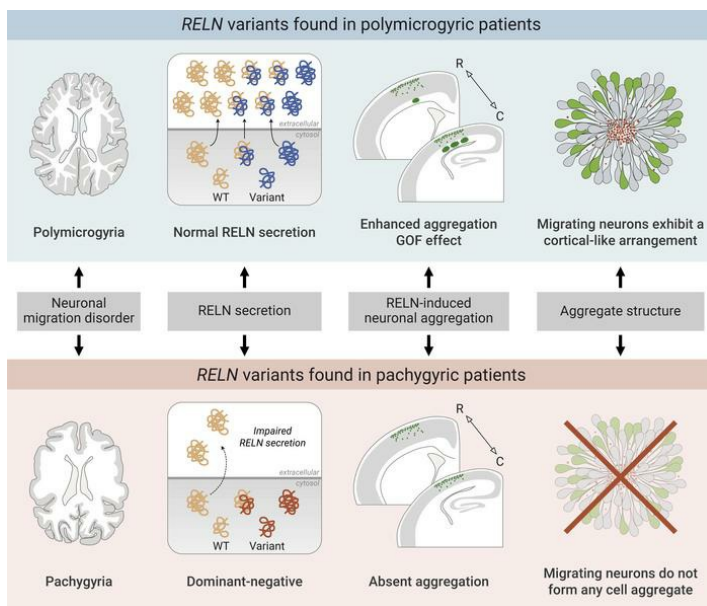# De novo monoallelic Reelin missense variants act in a dominant-negative manner causing neuronal migration disorders

Martina Riva, … , Nadia Bahi-Buisson, Alessandra Pierani

Research | In-Press Preview | Development | Neuroscience

Graphical abstract

1 **De novo monoallelic Reelin missense variants act in a dominant-negative manner causing**

2 **Neuronal Migration Disorders**

3

Martina Riva[1,2]†, Sofia Ferreira[1,2]†, Kotaro Hayashi[3]‡, Yoann Saillour[1,2]‡, Vera P. Medvedeva[1,2], Takao Honda[3], Kanehiro Hayashi[3], Claire Altersitz[1,2], Shahad Albadri[4], Marion Rosello[4], Julie Dang[4], Malo Serafini[4], Frédéric Causeret[1,2], Olivia J. Henry[5], Charles-Joris Roux[6], Céline Bellesme[7], Elena Freri[8], Dragana Josifova[9], Elena Parrini[10], Renzo Guerrini[10,11], Filippo Del Bene[4]§, Kazunori Nakajima[3]§, Nadia Bahi-Buisson[1,2]§ and Alessandra Pierani[1,2,12,13]∗

4

5 [1]Université Paris Cité, Institute of Psychiatry and Neuroscience of Paris (IPNP), INSERM

6 U1266, Team Genetics and Development of the Cerebral Cortex, F-75014 Paris, France.

7 [2]Université Paris Cité, Imagine Institute, Team Genetics and Development of the Cerebral

8 Cortex, F-75015, Paris, France.

9 [3]Department of Anatomy, Keio University School of Medicine, Tokyo 160-8582, Japan.

10 [4]Sorbonne Université, INSERM U968, CNRS UMR 7210, Institut de la Vision, Paris, France.

11 [5]Department of Molecular Medicine and Surgery, Karolinska Institute, Stockholm, Sweden.

12 [6]Pediatric Radiology, Necker Enfants Malades University Hospital, Université de Paris, Paris

13 France.

14 [7]Pediatric Neurology, Bicêtre University Hospital, Université Paris Saclay, Kremlin-Bicêtre,

15 France.

16 [8]Dipartimento di Neuroscienze Pediatriche Fondazione Istituto Neurologico "C. Besta",

17 Milano, Italy.

18 [9]Department of Clinical Genetics, Guy's and St. Thomas Hospital NHS Trust, London, United

19 Kingdom.

20 [10]Neuroscience Department, Meyer Children's Hospital IRCCS, Florence, Italy.

21 [11]University of Florence, Florence, Italy.

22 [12]Institut des Sciences Biologiques, Centre National de la Recherche Scientifique, Paris, France.

23 [13]GHU-Paris Psychiatrie et Neurosciences, Hôpital Sainte Anne, F-75014 Paris, France.

24

25 † These authors contributed equally to this work

26 ‡ These authors contributed equally to this work

27 § These authors contributed equally to this work

28 * Corresponding author: alessandra.pierani@inserm.fr

29 **ABSTRACT**

30

31 Reelin (RELN) is a secreted glycoprotein essential for cerebral cortex development. In humans,

32 recessive *RELN* variants cause cortical and cerebellar malformations, while heterozygous

33 variants were associated to epilepsy, autism and mild cortical abnormalities. However, their

34 functional effects remain unknown. We identified inherited and de novo *RELN* missense

35 variants in heterozygous patients with neuronal migration disorders (NMDs) as diverse as

36 pachygyria and polymicrogyria. We investigated in culture and in the developing mouse

37 cerebral cortex how different variants impacted RELN function. Polymicrogyria-associated

38 variants behaved as gain-of-function showing an enhanced ability to induce neuronal

39 aggregation, while those linked to pachygyria as loss-of-function leading to defective neuronal

40 aggregation/migration. The pachygyria-associated de novo heterozygous *RELN* variants acted

41 as dominant-negative by preventing wild-type RELN secretion in culture, animal models and

42 patients, thereby causing dominant NMDs. We demonstrated how mutant RELN proteins in

43 vitro and in vivo predict cortical malformation phenotypes, providing valuable insights into the

44 pathogenesis of such disorders.

INTRODUCTION

The neocortex is composed of six layers that are built during embryonic development through highly orchestrated processes of successive generation of cohorts of glutamatergic neurons in the proliferative zones and their radial migration to form distinct layers (1). The inside-out sequence in the formation of these layers, whereby later-born neurons bypass earlier-born ones to position more superficially, is a unique characteristic of the mammalian neocortex (2). This process relies on the first generated neurons, Cajal-Retzius cells (CRs), which from the cortical surface orchestrate the radial migration, through the secretion of the Reelin (RELN) protein (3, 4). RELN is a large secreted glycoprotein, which is cleaved in the extracellular environment at two main specific sites, between repeats 2-3 (N-t site) and repeats 6-7 (C-t site) (5-8), by cleaving enzymes such as matrix metalloproteinases (6, 9-11). Studies on RELN proteolysis have identified three key domains. The N-terminal (N-t) domain is necessary for multimerization (12, 13), while the central region (R3-6) binds to RELN receptors, apolipoprotein E receptor 2 (ApoER2) and very low density lipoprotein receptor (VLDLR) (5, 14-16). The C-terminus (C-t) contains a small carboxy-terminal region (CTR) and is required for downstream signaling activation (17, 18) but its role in secretion is not fully elucidated yet (18, 19). The full-length protein is generally more efficient in activating the transduction cascade probably due to the N-t region that promotes homodimerization through disulfide linkage, and the CTR that mediates proper folding (12, 13, 18, 20). Although RELN has been studied for almost three decades, its functions are still unclear. On one hand, it is proposed that it acts as an attractant cue (21), and on the other hand it is thought to serve as a "detach and go" signal instructing migrating neurons close to the marginal zone (MZ) to disengage from the radial glia and switch from a locomotion mode of migration to terminal translocation (5, 22-27). RELN has been initially studied via the characterization of the *reeler* (*rl/rl*) homozygous mouse mutant (4, 28), which shows a profound disorganization of cortical lamination, largely due to impaired migration of pyramidal neurons (3, 29). At the opposite, heterozygous *reeler* (*rl/+*) mice (haploinsufficient for RELN) show no defects in cortical layering but exhibit a spectrum of cognitive and behavioral abnormalities (30, 31), which emphasizes the relevance of RELN expression levels in higher brain functions.

In humans, recessive *RELN* variants in the homozygous or compound heterozygous state are associated to different patterns of lissencephaly (LIS) with cerebellar hypoplasia (LCH), a severely disabling developmental disorder (32-39), often linked with epilepsy. Fifteen pathogenic or likely pathogenic *RELN* variants in twelve families with this condition have been

79   identified to date, including null alleles, splice-site and missense variants. In addition, one

80   single patient with polymicrogyria, microcephaly and epilepsy was described with two

81   missense variants (40). Several heterozygous *RELN* variants were identified as risk factors for

82   multiple neuropsychiatric and neurodegenerative disorders, such as schizophrenia, bipolar

83   disorders, Autism Spectrum Disorders (ASD) and Alzheimer's disease (41-43) in the absence

84   of cortical malformations. Moreover, heterozygous *RELN* variants account for 17.5% of

85   familial cases of autosomal dominant lateral temporal lobe epilepsy (ADLTE) with relatively

86   low penetrance (44, 45). These are mainly missense variants, which alter structurally important

87   amino acids (aa) predicted to perturb protein folding (44, 45) but they do not lead to brain

88   malformations. Only four ADLTE-causing missense *RELN* variants (46) and one de novo

89   missense variant identified in an ASD patient (47) were functionally characterized in vitro

90   showing reduced secretion of mutated RELN. Recently, monoallelic *RELN* variants were

91   reported in eight families with frontotemporal or temporal-predominant LIS, but with normal

92   cerebellum and these include splice-site and missense variants (37, 48). However, it is unknown

93   whether the phenotypes arise from gain-of-function (GOF) or loss-of-function (LOF) and,

94   importantly, which specific sub-function of RELN may be affected in order to cause such high

95   variety of pathologies.

96   Here we report six patients with inherited and de novo heterozygous missense *RELN* variants

97   associated with a spectrum of malformations of cortical development (MCDs), namely

98   polymicrogyria (excessive number of abnormally small gyri) or pachygyria (simplified cortical

99   gyral pattern with shallow sulci and broad gyri) (49) without cerebellar hypoplasia. We

100   functionally characterized each variant through a set of in vitro and in vivo assays to assess the

101   secretion of the mutated proteins and their capacity to cause aggregates/rosettes and regulate

102   neuronal migration upon their ectopic expression in the embryonic mouse cerebral cortex. We

103   assessed their pathogenicity, demonstrating that all variants interfere with at least one of the

104   studied processes, and characterizing to what extent that interference correlates with the

105   pathological phenotype. We also provide what we believe to be the first evidence that

106   monoallelic de novo *RELN* variants found in pachygyria patients can cause autosomal dominant

107   NMDs by behaving as dominant-negative forms on wild-type (WT) RELN secretion in vitro,

108   in animal models and in patients. Our findings indicate that defects of RELN secretion and

109   function contributes to NMDs, shedding light on the involvement of RELN in the etiology of

110   MCDs.

RESULTS

Cortical malformations in patients carrying *RELN* variants

Seven missense *RELN* (NM_005045.4) variants were identified in six children with cortical malformations without cerebellar abnormalities (Figure 1, Table 1 and Supplemental Figure 1). One child (C1) carries two variants, and the other five have monoallelic variants: two brothers (MI1/2) bearing the same maternally-inherited variant, one child (DN*) with a paternally-inherited plus a de novo variant on the same allele, and lastly two unrelated children (DN1, DN2) with de novo variants. Affected children were diagnosed at 1-8 years of age with hypotonia and cognitive developmental delays. The first patient C1 exhibited bilateral fronto-temporo-parietal polymicrogyria and periventricular nodular heterotopia at brain magnetic resonance imaging (MRI) (Figure 1A). Next Generation Sequencing (NGS) analysis of a dedicated panel of genes associated with MCDs revealed two missense *RELN* variants, c.5461T>C (p.Tyr1821His) in Reelin repeat (RR) 4 and c.3839G>A (p.Gly1280Glu) in RR3, denoted as Y1821H and G1280E, respectively (Figure 1B and Table 1). The G1280E substitution was maternally inherited whereas Y1821H was de novo, but given the unavailability of DNA samples from the trio during this study, the presence of the two variants on the same allele (as patient DN*) or on different alleles cannot be assessed. Patients MI1 and MI2, two brothers (hence referred as MI1/2), exhibited MRI imaging consistent with bilateral perisylvian polymicrogyria (Figure 1A). In these two patients, a NGS panel for genes associated with MCDs and intellectual disability revealed the c.2737C>T (p.Arg913Cys) missense substitution (R913C) in the RR2 of the *RELN* gene (Figure 1B and Table 1), which they both inherited from their apparently healthy, but unexamined, mother. No other variants of significance were identified by whole-exome sequencing (WES) in these brothers. The fourth patient (DN*), exhibiting bilateral pachygyria, which is part of the LIS spectrum, primarily manifested in the frontal regions (Figure 1A), underwent NGS analysis of MCDs genes. It revealed the c.1949T>G/c.1667A>T (p.Ile560Ser/p.Asp556Val) missense *RELN* variants (I650S/D556V) with the I650S localized in RR1 and the D556V in the N-terminus domain (Figure 1B and Table 1). Parental analysis revealed that both variants are in a cis configuration on the same paternal allele (see Supplemental Methods). The last two patients, hereafter DN1 and DN2, as reported previously (37), presented at the brain MRI bilateral pachygyria with simplified gyral pattern, notably frontotemporal-predominant in the case of DN1 and frontal-predominant for DN2, and becoming less severe posteriorly (Figure 1A). NGS analysis of a panel for MCDs genes identified in patient DN1 a de novo c.1615T>C (p.Cys539Arg) variant

(C539R) in the N-terminal of the *RELN* gene and a de novo c.9619C>T (p.Arg3207Cys) in DN2 (R3207C) located in RR8 (Figure 1B and Table 1). Most of the *RELN* variants were predicted to be damaging by two web-based programs (PolyPhen-2 and CADD scores) except the inherited I650S. The majority was also absent from a public reference population database (Genome Aggregation Database [gnomAD] v3.1.2 non-neuro), whereas the G1280E was present with a 1.2% frequency and the R913C with very low frequency (Table 1). According to the American College of Medical Genetics/Association of Molecular Pathology (ACMG/AMP) 2015 guidelines (50), all de novo variants were assessed as likely pathogenic (PS2+PM1+PM2+PP3), the G1280E as benign (PM1+BS1+BS2+BP6) and the R913C (PM1+PM2+PP3) and I650S (PM1+PM2) as variants of unknown significance (VUS) (Table 1). All patients had normal comparative genomic hybridization array (CGH-Array). With the exception of MI1/2, all patients were born from non-consanguineous healthy parents. Among all patients, only MI1 had epilepsy. All family pedigrees are shown in Supplemental Figure 1.

These results suggest that heterozygous *RELN* variants are associated with a variety of cortical malformations, as diverse as pachygyria, which is a generalized transmantle migration abnormality, or polymicrogyria, which is still classified as a post-migrational disorder (51), in the absence of cerebellar hypoplasia, previously thought to be the hallmark of RELN-dependent autosomal recessive LIS.

RELN missense variants reduce its secretion

We first investigated whether the missense variants identified in the six patients with MCDs could affect RELN expression and/or secretion. We introduced each of the seven missense variants into the mouse *RELN* sequence (affected residues are conserved but shifted +1aa compared to human; see Supplemental Methods). IRES-eGFP-expressing plasmids carrying the mouse WT-RELN or the different variants were transfected into HEK293T cells, which lack endogenous RELN. RELN levels in both cell lysates and media were compared by immunoblotting using G10 (Figure 2) and 12/14 (Supplemental Figure 2) antibodies, recognizing epitopes in the N-t and C-t region, respectively (52). GFP-transfected cells showed no signal either in cell lysates or media (data not shown). Upon WT-RELN transfection, a single full-length (FL) 450 kDa band was observed in the cell fraction (Figure 2B), whereas the FL 450 kDa, the two complementary fragments resulting from the N-t cleavage NR2 (150 kDa) and R3-8 (250 kDa), and those resulting from the C-t cleavage NR6 (340 kDa) and R7-8 (80 kDa), were visible in the secreted fraction (Figures 2A, C and Supplemental Figure 2),

178   indicating that WT-RELN is efficiently secreted and processed as expected (53). In cell lysates,

179   significantly increased levels of FL RELN (450 kDa) were observed for I650S-, D556V-,

180   C539R- and R3207C-transfected cells compared to WT (Figure 2B). In contrast, we observed

181   a 40% decrease of RELN in the media of R913C-transfected cells, and a 48% and 78%

182   reduction in the media of I650S- and D556V-transfected cells, respectively (Figure 2C). A

183   stronger effect was observed for the C539R and R3207C variants for which both FL and all

184   RELN proteolytic fragments were undetectable in the culture media (Figure 2C). Similar

185   changes in secreted RELN caused by the different variants were detected using the 12/14

186   antibodies that recognize the C-terminal region of the protein (Supplemental Figure 2B).

187   Taken together, these observations indicate that the de novo variants in the patients with

188   pachygyria and the inherited variants in MI1/2 and DN* patients cause, respectively, strong and

189   mild deficiency in RELN secretion. The significant accumulation of intracellular RELN

190   detected for the I650S, D556V, C539R and R3207C variants is consistent with their pronounced

191   deficit in RELN secretion.

192

193   ***RELN* variants affect neuronal aggregation along the rostro-caudal axis of the developing**

194   **cerebral cortex**

195   RELN is important to regulate neuronal migration and positioning of migrating neurons

196   (3, 4). To test whether *RELN* variants affect its activity in vivo compared to their WT

197   counterpart, we took advantage of a functional assay developed by Kubo *et al*. (54). Ectopic

198   RELN expression in the developing cortex of mouse embryos drives the radial migration of

199   glutamatergic neurons to form cell aggregates organized around a RELN-rich center mimicking

200   its production by CRs in the MZ. We electroporated IRES-eGFP-expressing plasmids carrying

201   WT-RELN or the different variants in the embryonic mouse cortex at E14.5 and collected the

202   brains at postnatal day 1 (P1) (Figure 3A). As previously shown (54), we confirmed that WT-

203   RELN is capable to cause the formation of aggregates (Figure 3B). In addition, we found that

204   these were not forming randomly along the rostro-caudal axis, but exclusively in intermediate

205   and caudal regions along the rostro-caudal axis at hippocampal levels (*n*=6 WT) (Figure 3C).

206   Different effects were obtained when RELN variants were electroporated. I650S and D556V,

207   identified in the DN* patient with pachygyria, behaved as the WT with GFP$^+$ aggregates

208   forming caudally, although with a lower frequency (I650S: 3/9 and D556V: 3/5 brains with

209   aggregates), while the Y1821H, G1280E and R913C variants associated to polymicrogyria

210   promoted the formation of aggregates at both caudal and rostral levels (Figure 3B-C).

Interestingly, the C539R and R3207C variants, found in patients DN1 and DN2, failed to form cell aggregates, consistent with their severely impaired secretion (Figure 2B). All aggregates formed in the intermediate zone (IZ) just below the cortical plate (CP) labeled by TBR1, a marker of deep-layer neurons at this age (Supplemental Figure 3).

Overall, these results allowed to conclude that: i) aggregates are mostly obtained in posterior regions, indicating that different areas of the developing cortex are not equally responsive to ectopic RELN; ii) variants from C1, MI1/2 and DN* patients lead to the formation of aggregates in the posterior cortex, indicating that they retain some of the activity of the WT protein; iii) polymicrogyria-associated variants from C1 and MI1/2 patients appear to gain the capacity to induce aggregate formation at rostral levels (>50% of brains) and thus represent a GOF in this assay; iv) the two de novo variants from DN1 and DN2 patients behave as complete LOF as shown by the absence of aggregate formation.

Pachygyria-associated *RELN* missense variants fail to form properly well-organized rosettes

As previously detailed (54), upon WT-RELN electroporation into the developing mouse neocortex at E14.5, spheroid structures are observed at P1.5. These structures, which will be referred to as rosettes, feature electroporated cells projecting radially their processes towards a cell-body poor central region accumulating the RELN protein (Figures 4 and Supplemental Figure 4), analogously to the MZ of the developing cortex. Later-born neurons migrate through early-born neurons to reach the most internal part of this structure, recapitulating, even if ectopically, the inside-out development of the neocortex (54). About 44% of the WT aggregates (12/27) quantified along the rostro-caudal axis of the electroporated brains displayed a rosette structure (Table 2). We thus investigated whether the different missense variants driving the formation of aggregates could effectively generate well-structured rosettes. Our analysis focused on comparing the caudal aggregates obtained with the variants versus the ones induced by WT-RELN. The polymicrogyria-associated variants Y1821H, G1280E and R913C were the only variants generating rosettes with a cell body-poor center, respectively, 33%, 46% and 29% of the time (Figures 4, Table 2 and Supplemental Figure 4). Notably, these variants also exhibited a higher propensity for inducing neuronal aggregation compared to WT-RELN. This was evidenced not only by the rostral aggregation in over 50% of electroporated brains (Figure 3C), not observed with the WT protein, but also by the strong increase in the average number of aggregates found per brain (Table 2). However, regarding the genetic context of patient C1,

we observed that the de novo Y1821H variant seems to have a more pronounced effect on RELN function compared to the G1280E variant. It induced a higher number of aggregates per brain (16.1 *vs* 12.0), but with a lower proportion of rosettes (33% *vs* 46%) (Table 2). Conversely, I650S and D556V variants identified in the DN* pachygyria patient drove the formation of cell structures in which the GFP^{+} cells were spread throughout with their processes clearly misoriented, and, although expressing RELN, the mutant protein failed to accumulate in a central region (Figure 4 and Supplemental Figure 4). This resulted in structures completely lacking organization and cell body-sparse centers, which we defined simply as aggregates. Moreover, these variants displayed a lower capacity to induce neuronal aggregates, as indicated by the reduced number of aggregates per brain (Table 2), and did not form aggregates rostrally. Finally, cells electroporated with the C539R and R3207C variants expressed RELN but they were unable to cause any sort of aggregate and some GFP^{+} cells appeared arrested in the VZ (Figures 4, Table 2 and Supplemental Figure 4). Some of these neurons exhibited abnormal high levels of RELN intracellularly (Figure 4, white arrows), confirming the impairment of secretion detected in vitro (Figure 2B). All cell aggregates, whether affected or not, primarily consisted of later-born neurons expressing BRN2 destined to superficial layers (Supplemental Figures 3 and 4), in accordance with the stage of electroporation and consistent with prior reports (54).

We conclude that all polymicrogyria-associated variants (Y1821H, G1280E and R913C) can normally induce well-organized rosettes and are more prone to cause neuronal aggregation both caudally and rostrally. In contrast, variants associated with pachygyria (I650S, D556V, C539R and R3207C) behave as LOF by altering the formation of rosettes or even aggregates to different extents, ranging from structures lacking organization and cell body-poor centers (I650S and D556V in DN*) to the complete absence of neuronal aggregation (variants in DN1 and DN2 patients).

RELN variants alter neuronal migration rostrally

At rostral levels, where rosettes are not normally forming, WT-RELN-expressing GFP^{+} cells migrated to colonize the upper layers (UL) by P1, in particular layer (L)II/III, accordingly to the stage of electroporation (E14.5) (Figure 5A). Radially migrating neurons do not naturally express RELN, thus we used these electroporated principal neurons at rostral levels as a heterologous system to investigate the specific cell-autonomous effects of the different *RELN* variants on their migration. We divided the cortical wall in 10 equal bins and quantified the

percentage of GFP⁺ cells per bin. Bin 1 corresponded to the MZ/LI, bin 2-4 to the UL, bin 5-7 to the deeper layers (DL), bin 8-9 to the IZ and bin 10 to the VZ. When WT-RELN was ectopically expressed, 90% of GFP⁺ pyramidal neurons were found within bin 2-3 (70% in bin 2 and 20% in bin 3), corresponding approximately to LII/III as expected by the stage of electroporation. The remaining 10% of GFP⁺ cells were spread in the other bins (Figure 5A-B). When testing the Y1821H and I650S variants, defects were observed in the migration of the electroporated cells within the UL, with significantly less cells in bin 2 and more in bin 3. In contrast, the G1280E and R913C variants promoted an increase in the percentage of GFP⁺ cells trailing specifically in bin 6 and 7/10, respectively, corresponding to DL and VZ, despite no significant decrease in the percentage of neurons able to reach the UL (Figure 5A-B). These findings indicate that the G1280E and R913C variants had a relatively milder impact compared to the Y1821H and I650S variants. The D556V and R3207C variants did not affect the migration of the electroporated cells, thus behaving as the WT-RELN in this assay. The most striking effect was observed for the C539R variant, which strongly affected electroporated GFP⁺ cells with only 50% of them reaching the UL (bins 2-3) and the remaining being detected in deep locations, in particular in bins 7 to 10 (Figure 5A-B), corresponding to DL (layers V/VI), IZ and VZ.

To study whether disturbed migration was accompanied by changes in morphological features or fate we analyzed both the cells that were displaced in the CP and those able to reach the correct position in the UL. Mislocalized cells for all variants displayed a morphology of migrating neurons with a long apical process accumulating RELN (Supplemental Figure 5A). De novo D556V, C539R and R3207C variants appeared to cause an increased accumulation of RELN inside the cytoplasm of GFP⁺ cells (Supplemental Figure 5A white arrows) correlating with the in vitro observations (Figure 2B). Cells that were able to reach the UL for both WT-RELN and the different variants appeared to differentiate normally into pyramidal neurons having their dendrites in LI and accumulating RELN mainly in the primary apical dendrite (Supplemental Figure 5C). Both mislocalized GFP⁺ cells in the CP (Supplemental Figure 5B) and those arrived in the upper CP (Supplemental Figure 5D) maintained the identity of BRN2⁺ upper-layer neurons for every variant as for the WT-RELN showing that, even when mispositioned, electroporated cells maintained the correct upper-layer fate.

We conclude that the majority of variants alter cell-autonomously the migration of electroporated cells at rostral levels, although to different degrees, with the de novo C539R variant of DN1 being the most severely impaired.

Pachygyria-associated de novo heterozygous *RELN* variants behave as dominant-negative forms in vitro

To assess how RELN generated from mutant alleles might influence total RELN levels within the genetic context of the patients, we conducted in vitro co-transfections experiments using HEK293T cells. We replicated the heterozygous patients' genotype by co-transfecting WT-RELN with either the R913C, I650S/D556V (as carrying two variants in cis), C539R or R3207C variants for patients MI1/2, DN*, DN1 and DN2, respectively. For C1's two variants, we co-transfected Y1821H and G1280E to ascertain eventual combined effects on two different alleles. Western blot analysis of co-transfections mimicking C1 and MI1/2 genotypes showed unchanged amounts of RELN in both lysates and media (Figure 6A-B), while DN*, DN1 or DN2 variants displayed at least a 1.5 to 2-fold increase in intracellular levels (Figure 6A) and a strong reduction of more than 70% of total secreted RELN (Figure 6B) compared to WT controls. These results indicate that Y1821H and G1280E mutant proteins, when both present, are secreted as efficiently as WT proteins. As for the monoallelic heterozygous variants, the co-existence of the MI1/2 variant form with the WT-RELN protein did not change RELN secretion or its lysate levels, suggesting that this variant does not interfere with the WT protein. In contrast, the mutant carrying both I650S and D556V variants (I650S/D556V), and the C539R and R3207C variants seemed to strongly impair WT-RELN secretion while raising the amount of intracellular RELN (Figure 6A-B), suggesting a dominant-negative effect. To further address whether these secretion-defective *RELN* variants have a dominant-negative effect on the WT protein, a C-t Flag-tagged WT-RELN (20) (henceforth Flag-WT-RELN) was co-transfected with either unflagged WT-RELN or RELN-variants from the monoallelic heterozygous patients (MI1/2, DN*, DN1 and DN2). Western blotting with anti-Flag antibodies showed that the I650S/D556V, C539R and R3207C variants promoted a 80% decrease in secretion of Flag-WT-RELN (Figure 6D), consistent with a 2-fold accumulation of intracellular RELN (Figure 6C). The Flag-WT-RELN was identically secreted either when co-expressed with WT-RELN or the R913C variant (Figure 6D). Similar results were obtained when total RELN was detected using N-t anti-RELN G10 antibodies (Figure 6E-F). Altogether, these data demonstrate that the pachygyria-related variants generate secretion-defective RELN proteins that additionally act as effective dominant-negative in vitro.

To go further in the molecular mechanisms, we performed blots in non-reducing conditions to identify dimerized forms of RELN in co-expression experiments of Flag-WT-RELN and monoallelic variants. As expected (12), a high proportion of RELN proteins in the

media are present as dimers of around 900 kDa (Supplemental Figure 6A) and all monoallelic variants are capable to form dimers with WT-RELN extracellularly. Additionally, in all conditions, we observed the presence of what it seems to be RELN multimers in the cellular fraction unable to enter the SDS-PAGE gel (Supplemental Figure 6B). This indicates that RELN assembles into large protein complexes also intracellularly, suggesting a possible mechanism through which the pachygyria-associated variants I650S/D556V, C539R and R3207C retained the WT protein intracellularly (Figure 6C) and hindered its secretion (Figure 6D).

Pachygyria-associated de novo monoallelic *RELN* variants behave as dominant-negative in vivo in both animal models and patients

To assess the effect of *RELN* variants on its secretion in vivo we turned to animal models and focused on the variants acting as dominant-negative in vitro. Previous reports revealed the gradient distribution of the RELN protein in the zebrafish optic tectum and its critical role for lamina-specific axonal targeting (55). Thus, we generated a zebrafish model recapitulating the genotype of the DN2 patient. Upon introduction of the R3215C point mutation, corresponding to human *RELN* R3207C in DN2, RELN spatial distribution was analysed in 5 days post-fertilization embryos (Figure 7A-B). Anti-RELN immunostaining on tectal sections of R3215C wild-type siblings zebrafish embryos ($reln^{+/+}$) revealed the local enrichment of RELN at the basement membrane and a gradual decrease towards the periventricular (PV) zone of the neuropil (Figure 7A-B), similar as previously reported (55). In contrast, in $reln^{+/R3215C}$ and $reln^{R3215C/R3215C}$ mutants the RELN protein was detected in superficial interneurons (SINs), but a very weak or no clear extracellular localization of RELN could be detected in the heterozygotes and homozygotes, respectively, resulting in the abolishment of the gradient distribution of the protein (Figure 7A-B). This suggests a strong reduction of its secretion within the neuropil due to the introduction of the R3215C mutation. More importantly, the substantial ~80% decrease of RELN in the heterozygous $reln^{+/R3215C}$ aligns with the previous results obtained from the in vitro secretion assay (Figure 6B, D and F) and, thus, supports the dominant-negative effect of the human de novo R3207C variant also in vivo.

We were intrigued by the fact that, despite presenting pachygyria phenotypes, the single variants of the DN* patient did not exhibit defects in aggregate formation and secretion as severe as the two variants of DN1 and DN2 patients. We thus decided to model in mouse the de novo *RELN* D556V variant that was seen as the most defective based on the in vitro secretion

377 and in vivo aggregation assays compared to the coexisting I650S variant. We generated
378 heterozygous knock-in (KI) mice carrying the point *Reln* mutation D557V, corresponding to
379 the human D556V, and we found reduced extracellular RELN levels in the LI of *Reln*[+/D557V] P0
380 cerebral cortices (Figure 7C-D right graph). Consistently, the amount of intracellular RELN
381 was increased in the somata of p73[+] CRs (Figure 7C-D left graph), known to produce RELN in
382 the developing neocortex (3, 4). This in vivo model thus reaffirms the human D556V variant
383 as deleterious for RELN secretion in the cerebral neocortex. Given the co-occurrence of the de
384 novo D556V variant with the inherited I650S variant in cis on the same allele, which produced
385 a dominant-negative *RELN* variant in vitro (Figure 6), we sought to investigate whether the
386 I650S/D556V variant worsened the effect on RELN secretion and function. Indeed, its amount
387 was significantly raised in lysates of transfected HEK293T cells (Figure 7E) and totally absent
388 in the culture media (Figure 7F) compared to WT-RELN, aggravating secretion defects with
389 respect to each single variant alone (Supplemental Figure 7A-B). We next assessed whether the
390 I650S/D556V variant could prevent the capacity of RELN to form neuronal aggregates in vivo
391 when ectopically expressed in the developing mouse neocortex. We showed that electroporated
392 neurons with the I650S/D556V variant failed to cause neuronal aggregation in the IZ (Figure
393 7G-I) contrary to either the WT-RELN or even its single variants I650S and D556V, like what
394 observed for the C539R and R3207C variants (Figures 3 and 4). These results demonstrate that
395 RELN-dependent neuronal aggregation is abolished when both variants I650S and D556V co-
396 exist on the same protein, consistently with the strong dominant-negative behavior of the
397 I650S/D556V variant observed in vitro (Figure 6).

398   Finally, to analyze RELN secretion in humans we examined blood-serum RELN levels,
399 which is mostly secreted from the liver (56), from the DN* patient, the unaffected mother and
400 an unrelated control. The amount of the RELN fragment NR6, which is the most predominant
401 form in human (Supplemental Figure 7C), rat and mouse sera (56), was remarkably lower in
402 the serum of the DN* patient than in the sera from the healthy mother and control (Figures 7J
403 and Supplemental Figure 7D). In samples prior to several freeze-thaw cycles, full-length RELN
404 was also reduced in the affected child compared to the mother (Supplemental Figure 7D). The
405 lower levels of serum RELN indicate impaired liver secretion of the altered proteins, and
406 possibly reflects deficiency of secreted RELN in the brain of the DN* patient. We thus conclude
407 that the I650S/D556V variant is both a secretion-defective protein (Figure 7F) and a dominant-
408 negative RELN form (Figures 6B, D, F) in vitro and in vivo.

409

410   Collectively, these results show that *RELN* missense variants alter different aspects of
411   RELN secretion and function (Table 3). In particular, defects of in vitro⁄in vivo secretion and
412   in vivo regulation of neuronal aggregation and/or migration align with the phenotypic features
413   of the patients' malformations, providing molecular insights on the cause of a broad spectrum
414   of RELN-dependent NMDs. This functional characterization has contributed to improve the
415   pathogenicity score of all variants, according to the ACMG 2015 guidelines, as proposed and
416   summarized in Table 3.

DISCUSSION

RELN variants have been associated to a wide spectrum of neurodevelopmental disorders ranging from recessive forms of NMDs, namely LCH (57) with severe cerebral cortex and cerebellum malformations, to dominant ADLTE (44, 45), or psychiatric disorders such as autism and schizophrenia (41) with no apparent morphological brain abnormalities. Heterozygous *RELN* variants were also recently reported in individuals with mild LIS (37, 48), yet the underlying molecular mechanisms of such distinct pathological conditions remains unexplored. Here, we report six patients with heterozygous missense *RELN* variants, which expand the phenotypic spectrum of RELN-related cortical malformations to include pachygyria and polymicrogyria. Using complementary in vitro and in vivo assessments, we demonstrated that all heterozygous *RELN* missense variants linked to pachygyria severely prevented its secretion and neuronal aggregation activity, serving as causal to the disorder through a dominant-negative mechanism. Our findings also revealed that all tested polymicrogyria-associated variants maintained overall secreted RELN levels but presented an enhanced capacity to induce neuronal aggregation, suggesting their potential contribution to the pathology.

Among the six MCDs patients, three patients (DN*, DN1 and DN2) share a similar phenotype consisting of frontal-predominant pachygyria, characterized by a simplified gyral pattern with broad gyri due to incomplete transmantle migration (51). Our functional studies demonstrated that all *RELN* variants associated with pachygyria (I650S/D556V, C539R and R3207C) homogeneously behaved as LOF in the neuronal aggregation assay due to the severe impairment of their secretion. Indeed, high levels of secreted and functional RELN are required to induce ectopic rosettes with cell-body-sparse centers composed of leading processes and abundant extracellular RELN, similar to the MZ in vivo (54). These "mini-cortex"-like structures closely resemble the characteristic inside-out cell arrangement of the neocortex (54), which is determined by CRs secreting RELN in the MZ to control radial neuronal migration (3). The secretion analysis in vitro and in vivo further revealed a dominant-negative effect on the WT protein, supporting a pathogenic role of I650S/D556V, C539R and R3207C variants in causing a dominant form of pachygyria. The precise mechanism through which the mutant RELN proteins interfere with the WT protein remains undetermined. However, our immunoblotting results suggest that the presence of the mutant variants causes RELN retention in the intracellular compartment, possibly by "poisoning" the assembly of RELN multimers

15

inside the cells. This assembly-mediated dominant-negative effect is frequently observed for proteins that form homomeric complexes (58), as reported for secreted RELN (12). This negative dominance can particularly explain the difference between the DN* patient and the father, who carries the heterozygous I650S variant without any brain malformations. On one hand, the I650S variant alone, whose secretion was reduced to 50% in vitro, seems to be a benign variant concerning cortical malformations. Moreover, cortical layering in the heterozygous $Reln^{+/D557V}$ mouse (modeling the human de novo D556V) seemed typically normal despite the reduced levels of secreted RELN (70% secretion vs control) in the LI. This aligns with 50% of RELN being sufficient for a proper inside-out cortical lamination as observed in the heterozygous $reeler$ mouse (30) and ADLTE (44, 46) or ASD individuals (47) carrying heterozygous $RELN$ variants. On the other hand, both variants I650S and D556V showed partial LOF in the in vivo aggregation assay by resembling to the disorganized RELN-induced aggregates previously described in a knockdown model for Nrp1, a transmembrane protein that forms a complex with VLDLR to which RELN strongly binds (59). Taking all into account, it suggests that each individual variant could bind less efficiently to the Nrp1/VLDLR complex due to protein misfolding, but in isolation are insufficient to develop cortical malformations. Notably, we showed that the occurrence of pachygyria in the DN* child is caused by the dominant-negative effect of the I650S/D556V variant resulting from the synergistic interaction of the two variants that severely hampers RELN secretion to 20% when both present on the same allele as compared to their individual effects. This is indeed supported by the reduction of circulating RELN in the blood of the DN* patient. Lastly, this is what we believe to be the first study replicating human $RELN$ variants related to pathology in animal models. Both the KI $Reln^{+/D557V}$ mouse and $reln^{+/R3215C}$ zebrafish models showed in vivo alterations recapitulating the observed secretion deficiency of RELN in vitro and, more importantly, the mutant zebrafish, modeling the DN2 genotype (R3207C), revealed the damaging dominant-negative phenomenon of heterozygous variants in vivo, which severely drop RELN levels to 20%. Over the years, accumulating evidence has shown that RELN secreted by CRs concentrate in the MZ and is necessary in various developmental events during cortical lamination, beginning with the initial preplate splitting (60), and extending through multiple steps of radial glial-independent neuronal migration. The latter include somal translocation for early-born neurons (27), followed by multipolar migration (61, 62) and terminal translocation for late-born neurons (63). Disruptions at any RELN-dependent steps can result in cortical malformations (64). Hence, all evidences supporting the pathogenicity of $RELN$ variants identified in the pachygyria patients reflect deficient levels of functional RELN

in their developing neocortex that potentially disrupts RELN-dependent neuronal migration from its early steps.

The other three patients (C1 and MI1/2) presented different forms of bilateral polymicrogyria. Polymicrogyria is an etiologically heterogeneous malformation characterized by overfolding and dyslamination of the neocortex thought to arise from late migration deficits and/or post-migrational abnormalities (64). In contrast to pachygyria patients, the polymicrogyria-related variants Y1821H, G1280E and R913C revealed a GOF effect in our in vivo aggregation assay, firstly by promoting ectopic neuronal aggregation unusually in rostral brain regions, and secondly, by increasing aggregation caudally. These functional alterations seem unrelated to their secretion levels, as both Y1821H and G1280E variants with normal secretion, and the variant R913C with lower secretion levels (60%), similarly enhanced aggregation in vivo. Furthermore, they successfully induced well-structured rosettes with a central cell body-free MZ-like region. In the developing neocortex, RELN signals to late-born migrating cortical neurons when arrive beneath the MZ to organize the inside-out lamination (25) via an ApoER2-mediated mechanism regulating cell adhesion (61, 63, 65, 66), and to suppress neuronal invasion into the MZ via VLDLR (66, 67). These late developmental events are actually recapitulated in the RELN-induced aggregates, which involve both RELN receptors (54). This indicates that the binding to and signal transducing through ApoER2 and VLDLR receptors for all polymicrogyria-related variants should be intact. Nevertheless, all *RELN* variants displayed an enhanced rostro-caudal aggregation, shown to be facilitated by the direct promotion of N-cadherin-mediated cell adhesion of migrating neurons both during multipolar-bipolar transition and terminal translocation (65). This could suggest that the polymicrogyria-associated variants affect the adhesive properties of migrating neurons during possibly different steps of migration.

The R913C variant inherited from the mother, who has normal brain MRI but had epilepsy during childhood, was rare in gnomAD (~0.003%). Since WGS has yet to be performed for all polymicrogryria patients, the contribution of a deep intronic or regulatory variant in trans of the *RELN* variant or in another gene cannot be formally ruled out. However, NGS and WES did not identify additional variants in the MI1/2 brothers, which strongly reduces its probability. Concerning the Y1821H and G1280E variants in patient C1, the de novo occurrence of the Y1821H variant and its stronger associated effects in neuronal aggregation and migration compared to the G1280E variant allows the re-classification of Y1821H as pathogenic (Table 3) and suggests that it likely plays a critical role in the patient's phenotype.

17

Notably, the G1280E variant is proposed as VUS (Table 3) despite its functional alterations, due to its prevalence in around 1.2% of the normal population, with 11 reported homozygous individuals in the gnomAD (non-neuro) database (68), indicating that alone it is not sufficient to develop a pathological condition. However, we cannot exclude the possibility that the combined effect of the de novo Y1821H and inherited G1280E variants may contribute to the phenotype, irrespective of the allelic configuration of both variants. Nevertheless, our data showed that the variants found in patients with polymicrogyria function differently from the WT, likely by promoting excessive neuronal adhesion, but are not dominant negative, suggesting a contribution or predisposition to the manifestation of polymicrogyria in the patients rather than causality.

Many missense variants cause structural perturbations that may disrupt signal transduction through altered protein folding, protein-protein interactions, or receptor binding. In RELN, cysteine (Cys) residues are particularly important for both intramolecular disulfide bridges (69, 70) and homodimerization (13, 70), and three of the variants in this study involve cysteine-arginine interchanges. At the N-terminal region, which directs RELN non-covalent dimerization essential for its full biological activity, the C539R variant disrupts an intramolecular disulfide bond formed between the pair Cys^{462}-Cys^{539} (69), thus impairing this bridge and RELN's tertiary structure. Cys^{462} is left free to form new disulfide bonds and could interact with other Cys, including of the WT protein. The R913C and R3207C variants introduce new Cys in opposite domains of the protein, which could again affect correct folding and create new binding interfaces, such as intermolecular interactions with the WT protein. Nonetheless, the distinct phenotypes associated with R913C and R3207C variants pinpoint that an introduced Cys can actually generate opposite functional alterations, GOF or complete LOF, depending on protein domains, as demonstrated in this study. Regardless of their level of secretion, these aspects are crucial when exploring what is the significance of their intracellular and extracellular mechanisms of action to the associated pathology.

Our heterologous RELN expression assay in the developing mouse neocortex provided temporal and spatial control to assess the impact of all *RELN* variants on the radial migration of projection neurons without much interference from endogenous RELN. This assessment also allowed to track the migration of electroporated neurons from their birth in the VZ/SVZ to their final target position in the CP at rostral levels, in comparison to the WT counterpart. Our results showed that certain *RELN* variants led to the misplacement of electroporated neurons across

specific layers of the cortical wall. These observations suggest that missense variants can alter RELN function in neuronal migration in a cell-autonomous manner, a mechanism yet to be assessed in vivo within the naturally RELN-expressing neurons, notably CRs in the MZ and interneurons in the MZ, IZ and CP. The multiple roles of RELN signaling in neuronal migration seems to rely on the distinct expression patterns (71) and function of its ApoER2 and VLDLR receptors (61, 66, 67). However, in the case of polymicrogyria-associated variants, the canonical RELN signaling cascade involving ApoER2/VLDLR appears to be unaffected based on the well-organized rosettes formed. Consequently, misplacement of electroporated neurons within the cortical layers suggests that alternative signaling pathways could be impacted, involving other RELN-binding transmembrane proteins that have been proposed to participate in the regulation of RELN-dependent neuronal migration steps and cortical layering (72). These include $\beta 1$-containing integrins (23), and ephrins-B/EphB tyrosine kinase receptors (73, 74), which are differentially distributed along the migratory route (75-77). Further investigation is necessary to explore the effect of these pathology-associated variants on non-canonical RELN signaling that could be responsible for the mispositioning of the migrating neurons. Notably, our data revealed that the dominant-negative C539R variant (DN1) significantly affected the migration of electroporated cells rostrally, but the R3207C (DN2) did not. This disparity in effect appears to be independent of secretion, as both variants presented similar impairments in secreted levels, suggesting that their distinct effects on migration mostly occur in the intracellular milieu upon their expression. However, in case a small amount of protein is still secreted, we must also consider disparities in protein signaling due to the conformational differences caused by each amino acid substitution. Altogether, our observations highlight possible, yet unknown, protein-protein interactions between RELN and the migration machinery, and a potential cell-autonomous role in the distribution of RELN-producing cells, for instance for CRs, whose migration speed and consequent repartition in the developing neocortex are crucial for the patterning of higher-order cortical areas (78, 79).

None of the patients exhibited cerebellar anomalies previously shown as a hallmark of the *RELN*-associated LCH (57). Like in the homozygous *reeler* mouse (4), the majority of previously reported NMD patients with *RELN* variants (32-34) exhibit a severely hypoplastic cerebellum that is associated with complete absence of RELN caused by protein truncation or a null allele. We describe here missense variants with a full-length protein generated but with negative dominance in vitro and in vivo, which do not affect the cerebellum, thus suggesting that RELN levels around 20% are sufficient for cerebellar but not cerebral cortex development.

587   Notably, the heterozygous *reeler* mouse that has 50% reduction of RELN protein exhibits
588   altered cortical circuits without disturbed layering and is considered a model for schizophrenia
589   (30). Consistent with this observation, it was recently shown that half reduction of DAB1, an
590   essential downstream signaling molecule in RELN signaling, reduces the neocortical LI
591   thickness without defects in layer formation (80). Moreover, monoallelic missense *RELN*
592   variants with hampered secretion in heterologous cells in vitro were associated with ADLTE
593   (46) or ASD (47) without cortical malformations. Notably, ADLTE-linked variants impaired
594   trafficking of mutant RELN towards the secretory pathway, being degraded instead (46), but
595   the patients bearing the variants still showed significant levels of circulating RELN (44), which
596   does not support a dominant-negative effect. The ASD-related *RELN* variants also exhibited
597   decreased secretion without exerting a dominant negative effect on WT RELN secretion or
598   affecting the downstream RELN signaling cascade (47). A common mechanism was suggested
599   to underlie both RELN-dependent epilepsy and ASD and correlates with RELN
600   haploinsufficiency reducing protein levels to 50%, possibly explaining the insurgence of
601   ADLTE or psychiatric disorders in the absence of cortical morphological abnormalities. Our
602   work now shows that heterozygous *RELN* variants can lead to more severe phenotypes
603   accompanied by altered cortical organization, as observed in our patient cohort. This is
604   attributed to the dominant-negative effect of heterozygous *RELN* variants here observed that
605   will reduce secreted RELN levels to 20% in individuals with pachygyria (DN*, DN1 and DN2).
606   Finally, RELN secretion and thus overall WT RELN and mutant RELN levels are not perturbed
607   or mildly impaired (for the R913C variant) in polymicrogyria patients suggesting that proteins
608   levels are not contributing to the pathology. Together these results indicate that the occurrence
609   of pachygyria or polymicrogyria, epileptic and psychiatric conditions, depends on the
610   remaining distinct WT RELN levels as well as on the role of specific variants on protein
611   function.

612

613   In conclusion, we provide what we believe to be the first in vitro and in vivo functional
614   characterization of *RELN* missense variants associated with NMDs. The outcomes of our
615   functional studies allowed us to improve the pathogenicity scores for all tested variants,
616   proposing that all patients may carry either pathogenic or likely pathogenic *RELN* variants (see
617   Table 3) and further highlighted the relevance of circulating RELN levels for diagnosis. This
618   study paves the road for important functional assays for genotype-phenotype diagnostics to
619   understand the mechanistic involvement of future identified *RELN* variants in NMDs. We
620   correlate patients' phenotypes in the described polymicrogyria and pachygyria patients with

621   specific functional alterations of the RELN protein. Lastly, in addition to causing autosomal

622   recessive NMDs (32), our results demonstrate that *RELN* variants cause cortical malformations

623   also through dominant inheritance.

METHODS

Complete information on Methods is provided in Supplemental Methods.

Sex as a biological variable

Sex was not considered a biological variable. Both male and females animals were used in this study.

Statistics

Data are presented as mean $\pm$ SEM. Two-tailed one sample t test (hypothetical value of 1) after passing the Shapiro-Wilk normality test was used for statistical comparison of RELN levels obtained by western blotting. For the migration assay, the non-parametric Kolmogrov-Smirnov test to compare cumulative distributions was performed. RELN intensity in the KI mouse was evaluated using unpaired parametric 2-tailed Welch's t test, while the RELN gradient analysis in the larvae tectum used one-way ANOVA with Dunnett multiple comparisons as post-hoc test. Analyses were performed using GraphPad Prism 7.0 software. P values less than 0.05 were considered significant ($\star p<0.05$, $\star\star p<0.01$, $\star\star\star p<0.001$).

Study approval

Written and informed consent was obtained from all families prior to sample collection and processing. Animal procedures were performed in accordance with French and European Union animal welfare guidelines. In utero electroporation work was approved by the French Ministry of Higher Education, Research and Innovation as well as the Animal Experimentation Ethical Committee of Paris Descartes University (CEEA-34, licence numbers: 18011-2018012612027541 and 19319-2018020717269338), and zebrafish experiments were approved by committee on ethics of animal experimentation of Sorbonne Université (APAFIS#21323-2019062416186982). The mouse studies using the *Reln* D557V KI model were performed under the control of the Keio University Institutional Animal Care and Use Committee in accordance with the Institutional Guidelines on Animal Experimentation at the Keio University.

Data availability

All data are included in the article and supplemental material, and values for all data points are provided in the Supporting Data Values file. NGS data of two patients were deposited in the

658   Zenodo public database (accession: https://zenodo.org/records/11381515). Additional

659   information is available upon request from the corresponding clinician.

704

705   **Conflicts of interest:** The authors have declared that no conflict of interest exists.

REFERENCES

1. Rakic P, et al. Decision by division: making cortical maps. *Trends Neurosci*. May 2009;32(5):291-301.

2. Rakic P. Specification of cerebral cortical areas. *Science*. Jul 8 1988;241(4862):170-6. doi:10.1126/science.3291116

3. Ogawa M, et al. The reeler gene-associated antigen on Cajal-Retzius neurons is a crucial molecule for laminar organization of cortical neurons. *Neuron*. May 1995;14(5):899-912.

4. D'Arcangelo G, et al. A protein related to extracellular matrix proteins deleted in the mouse mutant reeler. *Nature*. Apr 20 1995;374(6524):719-23.

5. Jossin Y. Neuronal migration and the role of reelin during early development of the cerebral cortex. *Mol Neurobiol*. Dec 2004;30(3):225-51. doi:10.1385/MN:30:3:225

6. Lambert de Rouvroit C, et al. Reelin, the extracellular matrix protein deficient in reeler mutant mice, is processed by a metalloproteinase. *Exp Neurol*. Mar 1999;156(1):214-7. doi:10.1006/exnr.1998.7007

7. Koie M, et al. Cleavage within Reelin repeat 3 regulates the duration and range of the signaling activity of Reelin protein. *J Biol Chem*. May 2 2014;289(18):12922-30. doi:10.1074/jbc.M113.536326

8. Sato Y, et al. Determination of cleavage site of Reelin between its sixth and seventh repeat and contribution of meprin metalloproteases to the cleavage. *J Biochem*. Mar 2016;159(3):305-12. doi:10.1093/jb/mvv102

9. Krstic D, et al. Regulated proteolytic processing of Reelin through interplay of tissue plasminogen activator (tPA), ADAMTS-4, ADAMTS-5, and their modulators. *PLoS One*. 2012;7(10):e47793. doi:10.1371/journal.pone.0047793

10. Yamakage Y, et al. A disintegrin and metalloproteinase with thrombospondin motifs 2 cleaves and inactivates Reelin in the postnatal cerebral cortex and hippocampus, but not in the cerebellum. *Mol Cell Neurosci*. Oct 2019;100:103401. doi:10.1016/j.mcn.2019.103401

11. Hisanaga A, et al. A disintegrin and metalloproteinase with thrombospondin motifs 4 (ADAMTS-4) cleaves Reelin in an isoform-dependent manner. *FEBS Lett*. Sep 21 2012;586(19):3349-53. doi:10.1016/j.febslet.2012.07.017

12. Kubo K, et al. Secreted Reelin molecules form homodimers. *Neurosci Res*. Aug 2002;43(4):381-8. doi:10.1016/s0168-0102(02)00068-8

13. Utsunomiya-Tate N, et al. Reelin molecules assemble together to form a large protein complex, which is inhibited by the function-blocking CR-50 antibody. *Proc Natl Acad Sci U S A*. Aug 15 2000;97(17):9729-34. doi:10.1073/pnas.160272497

14. D'Arcangelo G, et al. Reelin is a ligand for lipoprotein receptors. *Neuron*. Oct 1999;24(2):471-9.

743   15.   Hiesberger T, et al. Direct binding of Reelin to VLDL receptor and ApoE receptor 2
744   induces tyrosine phosphorylation of disabled-1 and modulates tau phosphorylation. *Neuron*.
745   Oct 1999;24(2):481-9. doi:10.1016/s0896-6273(00)80861-2

746   16.   Trommsdorff M, et al. Reeler/Disabled-like disruption of neuronal migration in knockout
747   mice lacking the VLDL receptor and ApoE receptor 2. *Cell*. Jun 11 1999;97(6):689-701.
748   doi:10.1016/s0092-8674(00)80782-5

749   17.   Kohno T, et al. C-terminal region-dependent change of antibody-binding to the Eighth
750   Reelin repeat reflects the signaling activity of Reelin. *J Neurosci Res*. Nov 1 2009;87(14):3043-
751   53. doi:10.1002/jnr.22143

752   18.   Nakano Y, et al. The extremely conserved C-terminal region of Reelin is not necessary
753   for secretion but is required for efficient activation of downstream signaling. *J Biol Chem*. Jul
754   13 2007;282(28):20544-52. doi:10.1074/jbc.M702300200

755   19.   de Bergeyck V, et al. A truncated Reelin protein is produced but not secreted in the
756   'Orleans' reeler mutation (Reln[rl-Orl]). *Brain Res Mol Brain Res*. Oct 15 1997;50(1-2):85-90.

757   20.   Kohno T, et al. Importance of Reelin C-terminal region in the development and
758   maintenance of the postnatal cerebral cortex and its regulation by specific proteolysis. *J
759   Neurosci*. Mar 18 2015;35(11):4776-87. doi:10.1523/JNEUROSCI.4119-14.2015

760   21.   Gilmore EC, Herrup K. Cortical development: receiving reelin. *Curr Biol*. Feb 24
761   2000;10(4):R162-6. doi:10.1016/s0960-9822(00)00332-8

762   22.   Pinto-Lord MC, et al. Obstructed neuronal migration along radial glial fibers in the
763   neocortex of the reeler mouse: a Golgi-EM analysis. *Brain Res*. Aug 1982;256(4):379-93.
764   doi:10.1016/0165-3806(82)90181-x

765   23.   Dulabon L, et al. Reelin binds alpha3beta1 integrin and inhibits neuronal migration.
766   Research Support, Non-U.S. Gov't
767   Research Support, U.S. Gov't, P.H.S. *Neuron*. Jul 2000;27(1):33-44.

768   24.   Sanada K, et al. Disabled-1-regulated adhesion of migrating neurons to radial glial fiber
769   contributes to neuronal positioning during early corticogenesis. *Neuron*. Apr 22
770   2004;42(2):197-211. doi:10.1016/s0896-6273(04)00222-3

771   25.   Sekine K, et al. The outermost region of the developing cortical plate is crucial for both
772   the switch of the radial migration mode and the Dab1-dependent "inside-out" lamination in the
773   neocortex. *J Neurosci*. Jun 22 2011;31(25):9426-39. doi:10.1523/JNEUROSCI.0650-11.2011

774   26.   Borrell V, et al. In vivo evidence for radial migration of neurons by long-distance somal
775   translocation in the developing ferret visual cortex. *Cereb Cortex*. Nov 2006;16(11):1571-83.
776   doi:10.1093/cercor/bhj094

777   27.   Nadarajah B, et al. Two modes of radial migration in early development of the cerebral
778   cortex. *Nat Neurosci*. Feb 2001;4(2):143-50. doi:10.1038/83967

779   28.   Falconer DS. Two new mutants, 'trembler' and 'reeler', with neurological actions in the
780   house mouse (Mus musculus L.). *Journal of genetics*. Jan 1951;50(2):192-201.

781   29.   Tissir F, Goffinet AM. Reelin and brain development. *Nat Rev Neurosci*. Jun
782   2003;4(6):496-505.

783   30.   Tueting P, et al. The phenotypic characteristics of heterozygous reeler mouse.
784   *Neuroreport*. Apr 26 1999;10(6):1329-34.

785   31.   Qiu S, et al. Cognitive disruption and altered hippocampus synaptic function in Reelin
786   haploinsufficient   mice.   *Neurobiol   Learn   Mem*.   May   2006;85(3):228-42.
787   doi:10.1016/j.nlm.2005.11.001

788   32.   Hong SE, et al. Autosomal recessive lissencephaly with cerebellar hypoplasia is
789   associated with human RELN mutations. Research Support, Non-U.S. Gov't
790   Research Support, U.S. Gov't, P.H.S. *Nat Genet*. Sep 2000;26(1):93-6. doi:10.1038/79246

791   33.   Zaki M, et al. Identification of a novel recessive RELN mutation using a homozygous
792   balanced   reciprocal   translocation. *Am J Med Genet A*. May 1 2007;143A(9):939-44.
793   doi:10.1002/ajmg.a.31667

794   34.   Di Donato N, et al. Analysis of 17 genes detects mutations in 81% of 811 patients with
795   lissencephaly. *Genetics in medicine : official journal of the American College of Medical
796   Genetics*. Nov 2018;20(11):1354-1364. doi:10.1038/gim.2018.8

797   35.   Valence S, et al. RELN and VLDLR mutations underlie two distinguishable clinico-
798   radiological phenotypes. *Clin Genet*. Dec 2016;90(6):545-549. doi:10.1111/cge.12779

799   36.   Chang BS, et al. The role of RELN in lissencephaly and neuropsychiatric disease.
800   *American journal of medical genetics Part B, Neuropsychiatric genetics : the official
801   publication of the International Society of Psychiatric Genetics*. Jan 5 2007;144B(1):58-63.
802   doi:10.1002/ajmg.b.30392

803   37.   Di Donato N, et al. Monoallelic and biallelic mutations in RELN underlie a graded series
804   of   neurodevelopmental   disorders. *Brain*.   Sep   14   2022;145(9):3274-3287.
805   doi:10.1093/brain/awac164

806   38.   Igreja L, et al. Lissencephaly With Cerebellar Hypoplasia Due To a New RELN Mutation.
807   *Pediatr Neurol*. Dec 2023;149:137-140. doi:10.1016/j.pediatrneurol.2023.09.012

808   39.   Zillhardt JL, et al. Mosaic parental germline mutations causing recurrent forms of
809   malformations of cortical development. *European journal of human genetics : EJHG*. Apr
810   2016;24(4):611-4. doi:10.1038/ejhg.2015.192

811   40.   Wiszniewski W, et al. Comprehensive genomic analysis of patients with disorders of
812   cerebral cortical development. *European journal of human genetics : EJHG*. Aug
813   2018;26(8):1121-1131. doi:10.1038/s41431-018-0137-z

814   41.   Folsom TD, Fatemi SH. The involvement of Reelin in neurodevelopmental disorders.
815   Research Support, N.I.H., Extramural
816   Review. *Neuropharmacology*. May 2013;68:122-35. doi:10.1016/j.neuropharm.2012.08.015

817   42.   Lammert DB, Howell BW. RELN Mutations in Autism Spectrum Disorder. *Frontiers in
818   cellular neuroscience*. 2016;10:84. doi:10.3389/fncel.2016.00084

43.   Ishii K, et al. Reelin and Neuropsychiatric Disorders. Review. *Frontiers in cellular neuroscience*. 2016;10:229. doi:10.3389/fncel.2016.00229

44.   Dazzo E, et al. Heterozygous reelin mutations cause autosomal-dominant lateral temporal epilepsy. *American journal of human genetics*. Jun 4 2015;96(6):992-1000. doi:10.1016/j.ajhg.2015.04.020

45.   Michelucci R, et al. Autosomal dominant lateral temporal lobe epilepsy associated with a novel reelin mutation. *Epileptic Disord*. Aug 1 2020;22(4):443-448. doi:10.1684/epd.2020.1176

46.   Dazzo E, Nobile C. Epilepsy-causing Reelin mutations result in impaired secretion and intracellular degradation of mutant proteins. *Human molecular genetics*. Mar 3 2022;31(5):665-673. doi:10.1093/hmg/ddab271

47.   Lammert DB, et al. The de novo autism spectrum disorder RELN R2290C mutation reduces Reelin secretion and increases protein disulfide isomerase expression. *J Neurochem*. Jul 2017;142(1):89-102. doi:10.1111/jnc.14045

48.   Riva M, et al. Functional characterization of RELN missense mutations involved in recessive and dominant forms of Neuronal Migration Disorders. *bioRxiv*. 2021:2021.05.25.445586. doi:10.1101/2021.05.25.445586

49.   Oegema R, et al. International consensus recommendations on the diagnostic work-up for malformations of cortical development. *Nat Rev Neurol*. Nov 2020;16(11):618-635. doi:10.1038/s41582-020-0395-6

50.   Richards S, et al. Standards and guidelines for the interpretation of sequence variants: a joint consensus recommendation of the American College of Medical Genetics and Genomics and the Association for Molecular Pathology. *Genetics in medicine : official journal of the American College of Medical Genetics*. May 2015;17(5):405-24. doi:10.1038/gim.2015.30

51.   Barkovich AJ, et al. A developmental and genetic classification for malformations of cortical development: update 2012. *Brain*. May 2012;135(Pt 5):1348-69. doi:10.1093/brain/aws019

52.   de Bergeyck V, et al. A panel of monoclonal antibodies against reelin, the extracellular matrix protein defective in reeler mutant mice. *J Neurosci Methods*. Jul 1 1998;82(1):17-24. doi:10.1016/s0165-0270(98)00024-7

53.   Jossin Y, et al. Processing of Reelin by embryonic neurons is important for function in tissue but not in dissociated cultured neurons. *J Neurosci*. Apr 18 2007;27(16):4243-52. doi:10.1523/JNEUROSCI.0023-07.2007

54.   Kubo K, et al. Ectopic Reelin induces neuronal aggregation with a normal birthdate-dependent "inside-out" alignment in the developing neocortex. Research Support, Non-U.S. Gov't. *J Neurosci*. Aug 18 2010;30(33):10953-66. doi:10.1523/JNEUROSCI.0486-10.2010

55.   Di Donato V, et al. An Attractive Reelin Gradient Establishes Synaptic Lamination in the Vertebrate Visual System. *Neuron*. Mar 7 2018;97(5):1049-1062 e6. doi:10.1016/j.neuron.2018.01.030

858 56. Smalheiser NR, et al. Expression of reelin in adult mammalian blood, liver, pituitary pars
859 intermedia, and adrenal chromaffin cells. *Proc Natl Acad Sci U S A*. Feb 1 2000;97(3):1281-6.
860 doi:10.1073/pnas.97.3.1281

861 57. Kato M, Dobyns WB. Lissencephaly and the molecular basis of neuronal migration. *Hum*
862 *Mol Genet*. Apr 1 2003;12 Spec No 1:R89-96. doi:10.1093/hmg/ddg086

863 58. Bergendahl LT, et al. The role of protein complexes in human genetic disease. *Protein*
864 *Sci*. Aug 2019;28(8):1400-1411. doi:10.1002/pro.3667

865 59. Kohno T, et al. Reelin-Nrp1 Interaction Regulates Neocortical Dendrite Development in
866 a Context-Specific Manner. *J Neurosci*. Oct 21 2020;40(43):8248-8261.
867 doi:10.1523/JNEUROSCI.1907-20.2020

868 60. Sheppard AM, Pearlman AL. Abnormal reorganization of preplate neurons and their
869 associated extracellular matrix: an early manifestation of altered neocortical development in the
870 reeler mutant mouse. *J Comp Neurol*. Feb 10 1997;378(2):173-9. doi:10.1002/(sici)1096-
871 9861(19970210)378:2<173::aid-cne2>3.0.co;2-0

872 61. Hirota Y, et al. ApoER2 Controls Not Only Neuronal Migration in the Intermediate Zone
873 But Also Termination of Migration in the Developing Cerebral Cortex. *Cereb Cortex*. Jan 1
874 2018;28(1):223-235. doi:10.1093/cercor/bhw369

875 62. Jossin Y, Cooper JA. Reelin, Rap1 and N-cadherin orient the migration of multipolar
876 neurons in the developing neocortex. *Nat Neurosci*. Jun 2011;14(6):697-703.
877 doi:10.1038/nn.2816

878 63. Sekine K, et al. Reelin controls neuronal positioning by promoting cell-matrix adhesion
879 via inside-out activation of integrin alpha5beta1. *Neuron*. Oct 18 2012;76(2):353-69.
880 doi:10.1016/j.neuron.2012.07.020

881 64. Severino M, et al. Definitions and classification of malformations of cortical
882 development: practical guidelines. *Brain*. Oct 1 2020;143(10):2874-2894.
883 doi:10.1093/brain/awaa174

884 65. Matsunaga Y, et al. Reelin transiently promotes N-cadherin-dependent neuronal adhesion
885 during mouse cortical development. *Proc Natl Acad Sci U S A*. Feb 21 2017;114(8):2048-2053.
886 doi:10.1073/pnas.1615215114

887 66. Hack I, et al. Divergent roles of ApoER2 and Vldlr in the migration of cortical neurons.
888 *Development*. Nov 2007;134(21):3883-91. doi:10.1242/dev.005447

889 67. Hirota Y, Nakajima K. VLDLR is not essential for reelin-induced neuronal aggregation
890 but suppresses neuronal invasion into the marginal zone. *Development*. Jun 15
891 2020;147(12)doi:10.1242/dev.189936

892 68. Chen S, et al. A genomic mutational constraint map using variation in 76,156 human
893 genomes. *Nature*. Jan 2024;625(7993):92-100. doi:10.1038/s41586-023-06045-0

894 69. Nagae M, et al. Structural studies of reelin N-terminal region provides insights into a
895 unique structural arrangement and functional multimerization. *J Biochem*. Jul 3
896 2021;169(5):555-564. doi:10.1093/jb/mvaa144

897   70.   Yasui N, et al. Functional importance of covalent homodimer of reelin protein linked via
898   its central region. *J Biol Chem*. Oct 7 2011;286(40):35247-56. doi:10.1074/jbc.M111.242719

899   71.   Hirota Y, et al. Reelin receptors ApoER2 and VLDLR are expressed in distinct
900   spatiotemporal patterns in developing mouse cerebral cortex. *J Comp Neurol*. Feb 15
901   2015;523(3):463-78. doi:10.1002/cne.23691

902   72.   Alexander A, et al. Reelin through the years: From brain development to inflammation.
903   *Cell reports*. Jun 27 2023;42(6):112669. doi:10.1016/j.celrep.2023.112669

904   73.   Bouche E, et al. Reelin induces EphB activation. *Cell Res*. Apr 2013;23(4):473-90.
905   doi:10.1038/cr.2013.7

906   74.   Senturk A, et al. Ephrin Bs are essential components of the Reelin pathway to regulate
907   neuronal migration. *Nature*. Apr 21 2011;472(7343):356-60. doi:10.1038/nature09874

908   75.   Kischel A, et al. Ephrin-B2 paces neuronal production in the developing neocortex. *BMC
909   Dev Biol*. May 13 2020;20(1):12. doi:10.1186/s12861-020-00215-3

910   76.   Laussu J, et al. Beyond boundaries--Eph:ephrin signaling in neurogenesis. *Cell Adh Migr*.
911   2014;8(4):349-59. doi:10.4161/19336918.2014.969990

912   77.   Liebl DJ, et al. mRNA expression of ephrins and Eph receptor tyrosine kinases in the
913   neonatal and adult mouse central nervous system. *J Neurosci Res*. Jan 1 2003;71(1):7-22.
914   doi:10.1002/jnr.10457

915   78.   Barber M, et al. Migration Speed of Cajal-Retzius Cells Modulated by Vesicular
916   Trafficking Controls the Size of Higher-Order Cortical Areas. *Curr Biol*. Oct 5
917   2015;25(19):2466-78. doi:10.1016/j.cub.2015.08.028

918   79.   Griveau A, et al. A novel role for Dbx1-derived Cajal-Retzius cells in early
919   regionalization of the cerebral cortical neuroepithelium. *PLoS Biol*. 2010;8(7):e1000440.

920   80.   Honda T, et al. Heterozygous Dab1 Null Mutation Disrupts Neocortical and Hippocampal
921   Development. *eNeuro*. Apr 2023;10(4)doi:10.1523/ENEURO.0433-22.2023
922

1009 **Table 1. Recapitulative table of patients' genotype and phenotype with inheritance and pathogenicity score**

Patient	Nucleotide change	Variant	Segregation	Polyphen-2	CADD	ACMG class	gnomAD (non-neuro)	Published	Age of first assessment	Pathology
C1	c.5461T>C	Y1821H	de novo	0.983 PD	27.3	LP	0	No	13 months	Bilateral polymicrogyria, nodular heterotopia
	c.3839G>A	G1280E	maternal	0.997 PD	26.2	B	1617/134746 (11 Hom)	No		
MI1 MI2	c.2737C>T	R913C	maternal	0.988 PD	32	VUS	4/134700	No	4 years 14 months	Bilateral perisylvian polymicrogyria
DN*	c.1949T>G	I650S	paternal	0.261 B	24.7	VUS	0	No	16 months	Bilateral pachygyria
	c.1667A>T	D556V	de novo	0.994 PD	28.3	LP	0	No		
DN1	c.1615T>C	C539R	de novo	0.986 PD	24.9	LP	0	Yes	2 years	Bilateral pachygyria
DN2	c.9619C>T	R3207C	de novo	0.776 PsD	32	LP	0	Yes	2 years	Bilateral pachygyria

1010 CADD, Combined Annotation Dependent Depletion; ACMG, American College of Medical Genetics and Genomics; gnomAD, Genome

1011 Aggregation Database; PD, probably damaging; B, benign; PsD, possibly damaging; LP, likely pathogenic; VUS, variant of uncertain significance;

1012 Hom, homozygous.

1013

1014 **Table 2. Analysis of RELN-induced aggregates upon electroporation of WT-RELN and the different variants**

	WT	Y1821H	G1280E	R913C	I650S	D556V	C539R	R3208C
No. of brains	6	17	12	7	9	5	5	7
Total no. aggregates	27	224	129	75	7	11	0	0
No. aggregates/brain	4.5	16.1	12.0	12.0	0.8	2.2	0	0
With center (rosette)	44%	33%	46%	29%	14%	0%	NA	NA

1015 Quantification of the total number of aggregates, including per brain, and the percentage with a proper center (rosette structure). NA, not applicable.

1016

1017

1018

1019

32

Table 3. Summary of the performed assays

Patient	Variant	Secretion	Dominant neg.	Aggregate position	Structure	Migration	New ACMG class	Pathology
	WT	+		Caudal	✳			
C1	Y1821H	+	-	Rostral/Caudal	✳	≠ (UL)	P	Bilateral polymicrogyria, nodular heterotopia
	G1280E	+	-	Rostral/Caudal	✳	≠ (DL)	VUS	
MI1/2	R913C	↓↓↓	-	Rostral/Caudal	✳	≠ (VZ/DL)	LP	Bilateral perisylvian polymicrogyria
DN*	I650S	↓	-	Caudal	⬭	≠ (UL)	LP	
	D556V	↓↓	-	Caudal	⬭	=	P	Bilateral pachygyria
	I650S/D556V	↓↓↓	+	✗	✗	NA	P*	
DN1	C539R	↓↓↓	+	✗	✗	≠ (VZ/IZ/DL)	P	Bilateral pachygyria
DN2	R3207C	↓↓↓	+	✗	✗	=	P	Bilateral pachygyria

In vitro and in vivo assay results and correlation with patients' phenotypes. **+** Yes; **─** No; ↓ reduced; ↓↓ very reduced; ↓↓↓ severely reduced; ✳ rosette; ⬭ aggregate; **X** no aggregation; **=** not altered; **≠** altered; NA, not analyzed; UL, upper layers; DL, deeper layers; IZ, intermediate zone; VZ, ventricular zone; ACMG, The American College of Medical Genetics and Genomics; P, pathogenic; LP, likely pathogenic; VUS, variant of unknown significance. *authors' pathogenicity interpretation, as ACMG guidelines do not provide interpretation for monoallelic variants with two mutations in cis.
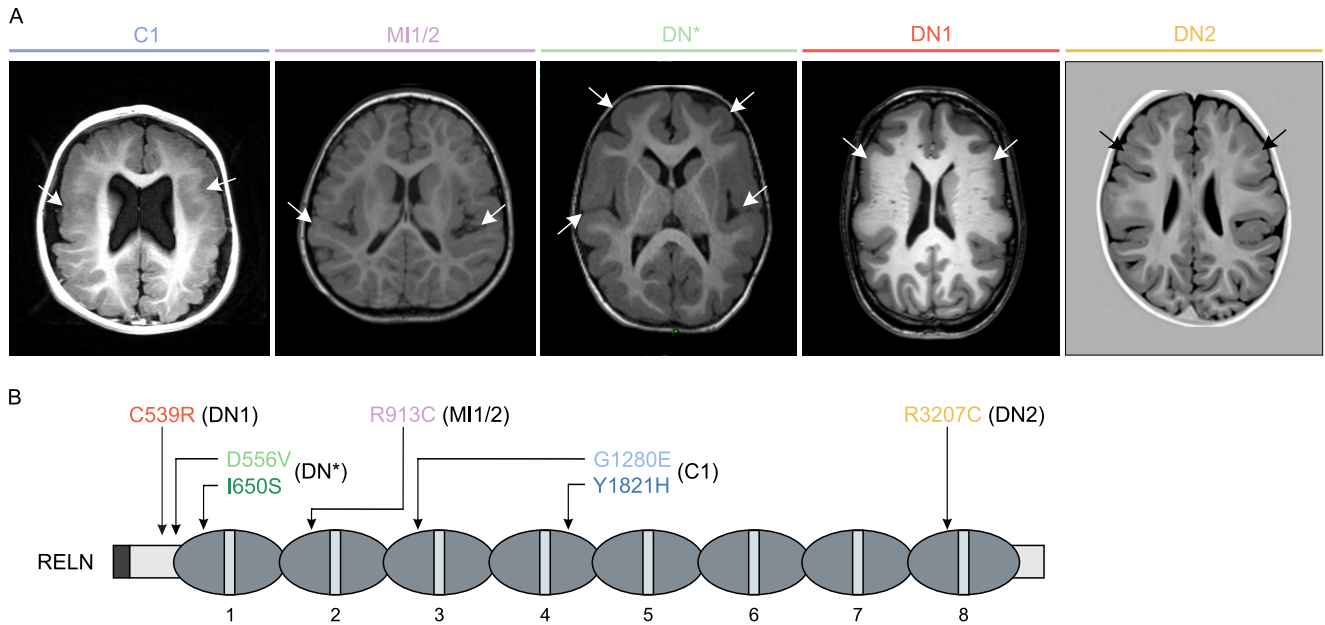
Figure 1. Cortical malformations in heterozygous patients associated with *RELN* missense variants. (A) Brain magnetic resonance imaging (MRI) from patients with heterozygous *RELN* variants. C1 exhibits bilateral fronto-parietal polymicrogyria with nodular heterotopia, MI1/2 bilateral perisylvian polymicrogyria, DN* frontal-predominant bilateral pachygyria, DN1 and DN2 frontotemporal-predominant bilateral pachygyria. Representative axial T1 section of the cortical malformations (white arrows). **(B)** Primary structure of the RELN protein showing eight reelin repeats (1-8 ovals). Arrows indicate the position of missense variants, each color corresponds to one patient (C1 blue, MI1/2 pink, DN* green, DN1 orange and DN2 yellow).
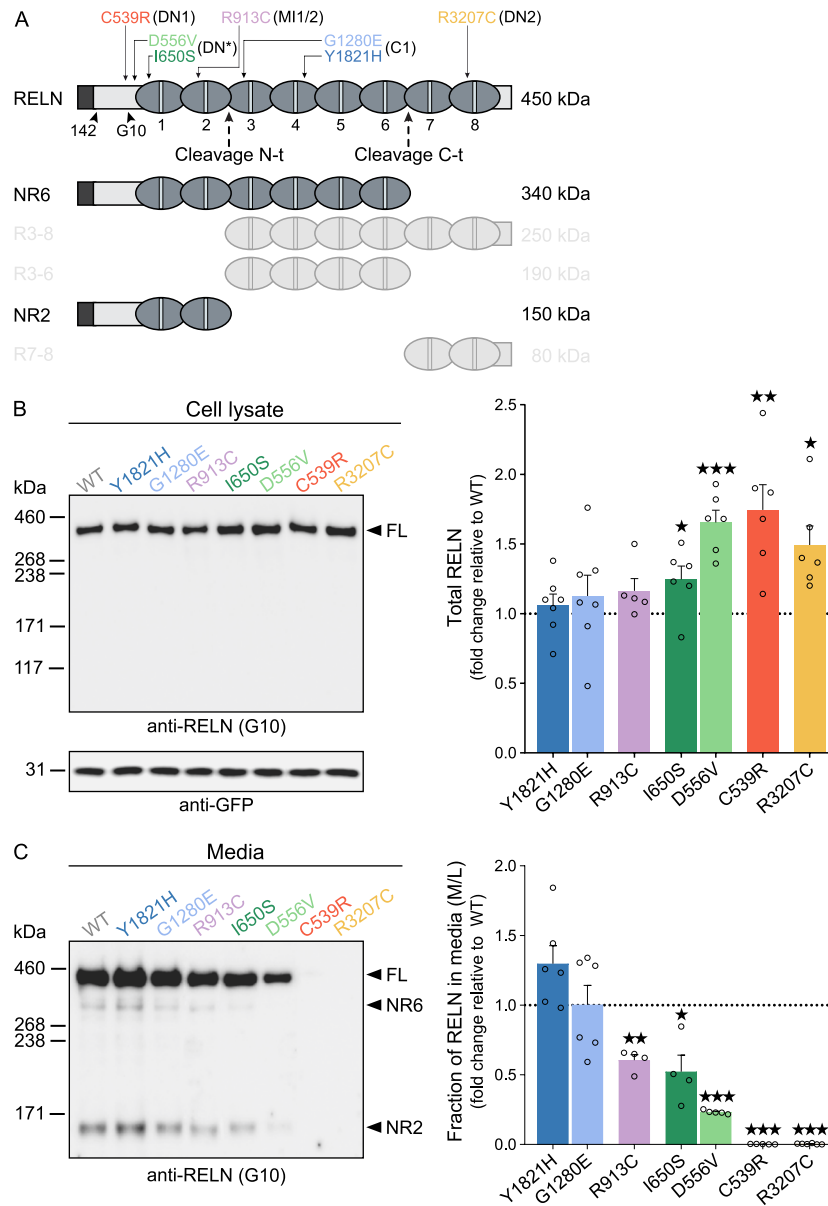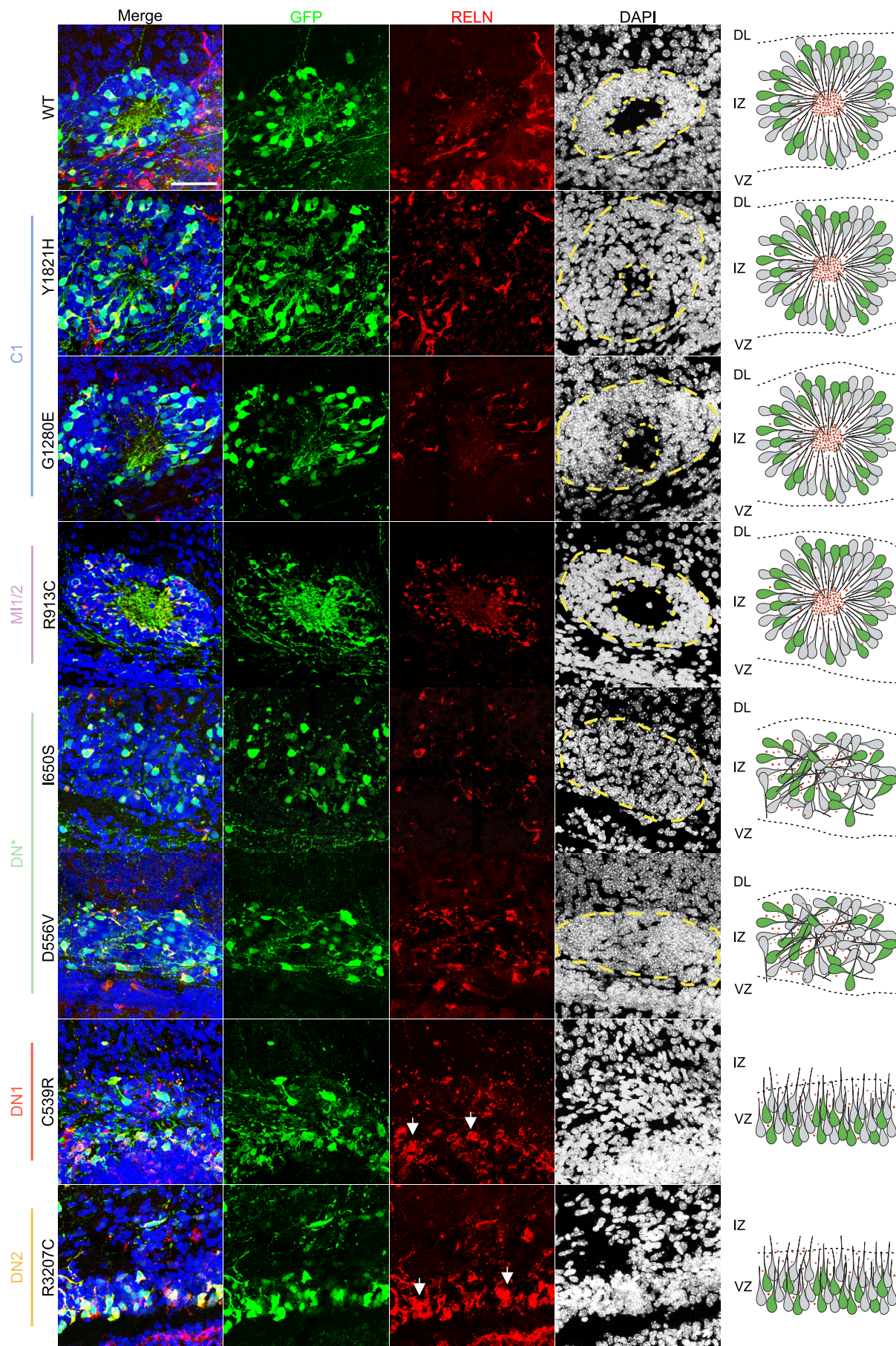
Figure 2. Missense variants alter RELN secretion in vitro. (A) Schematic of the full-length (FL) RELN protein (450 kDa), its N-t and C-t cleavage sites (dashed arrows), and its five cleaved products (NR6, R3-8, R3-6, NR2, R7-8). The binding regions of the 142 and G10 antibodies and the position of *RELN* variants in the patient color coding are indicated with arrowheads and arrows, respectively. **(B-C)** Immunoblottings (left) and densitometric analysis (right) of HEK293T cell lysates **(B)** and media **(C)** transfected with either WT-RELN or RELN-variants, probed with anti-RELN G10 or anti-GFP antibodies. RELN signal normalized to GFP in lysates (*n*=5-7 independent transfections) and expressed as the media (M)-to-lysate (L) ratio in the media (*n*=4-6 independent transfections). Data are mean ± SEM; 2-tailed one sample *t* test, ★$p<0.05$, ★★$p<0.01$, ★★★$p<0.001$. kDa, protein standard sizes.

Figure 3. *RELN* variants affect the capacity to form aggregates along the rostro-caudal axis in the embryonic mouse cortex. (A) Schematic representation of in utero electroporation (IUE) at E14.5 and collection at P1. **(B)** Wide-field immunofluorescence images of GFP[+] (green) aggregates (white arrowheads), with DAPI counterstaining (blue), at two rostro-caudal levels (Bregmas 0.86 and -1.58) of P1 mouse brains upon IUE of WT-RELN and patients' variants, Y1821H, G1280E, R913C, I650S, D556V, C539R and R3207C. Scale bar, 500 μm. **(C)** Quantification of aggregate formation at rostral and caudal levels for all electroporated constructs (*n*=3-17 electroporated brains per construct).
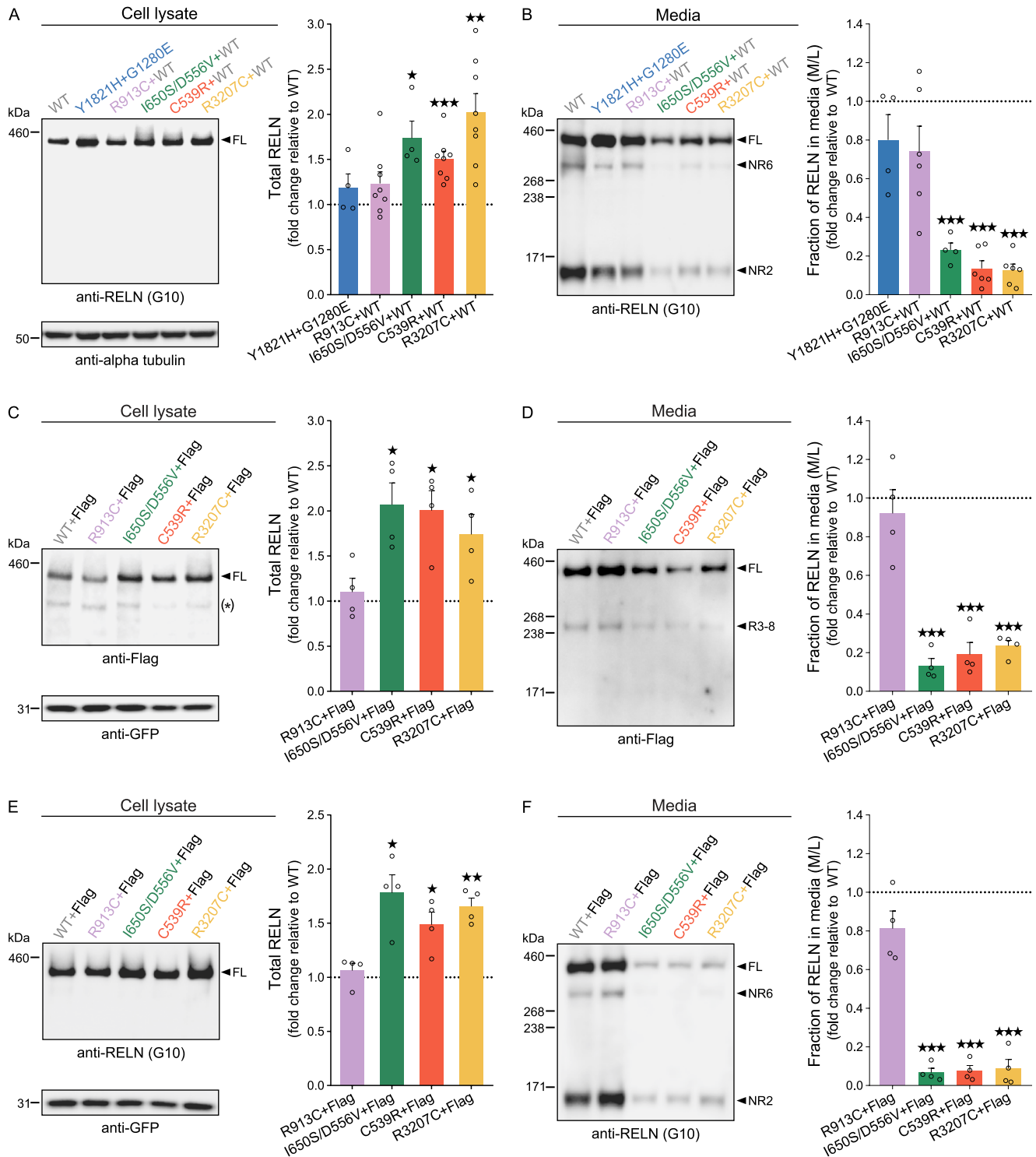
Figure 4. Pachygyria-associated variants fail to generate well-structured rosettes. Immunofluorescence images of aggregates stained with GFP (green) and RELN (red) antibodies and DAPI (blue) for nuclei. Aggregates with electroporated GFP+ cells projecting their processes toward a central region that is cell body-poor and RELN-rich are considered properly formed rosettes. Aggregates lacking a central cell-body-sparse region with the processes of GFP+ cells not projecting radially toward it are simply classified as aggregates. VZ, ventricular zone; IZ, intermediate zone; DL, deep layers. White arrows indicate GFP+ cells with increased RELN signal. Scale bar, 50 µm.
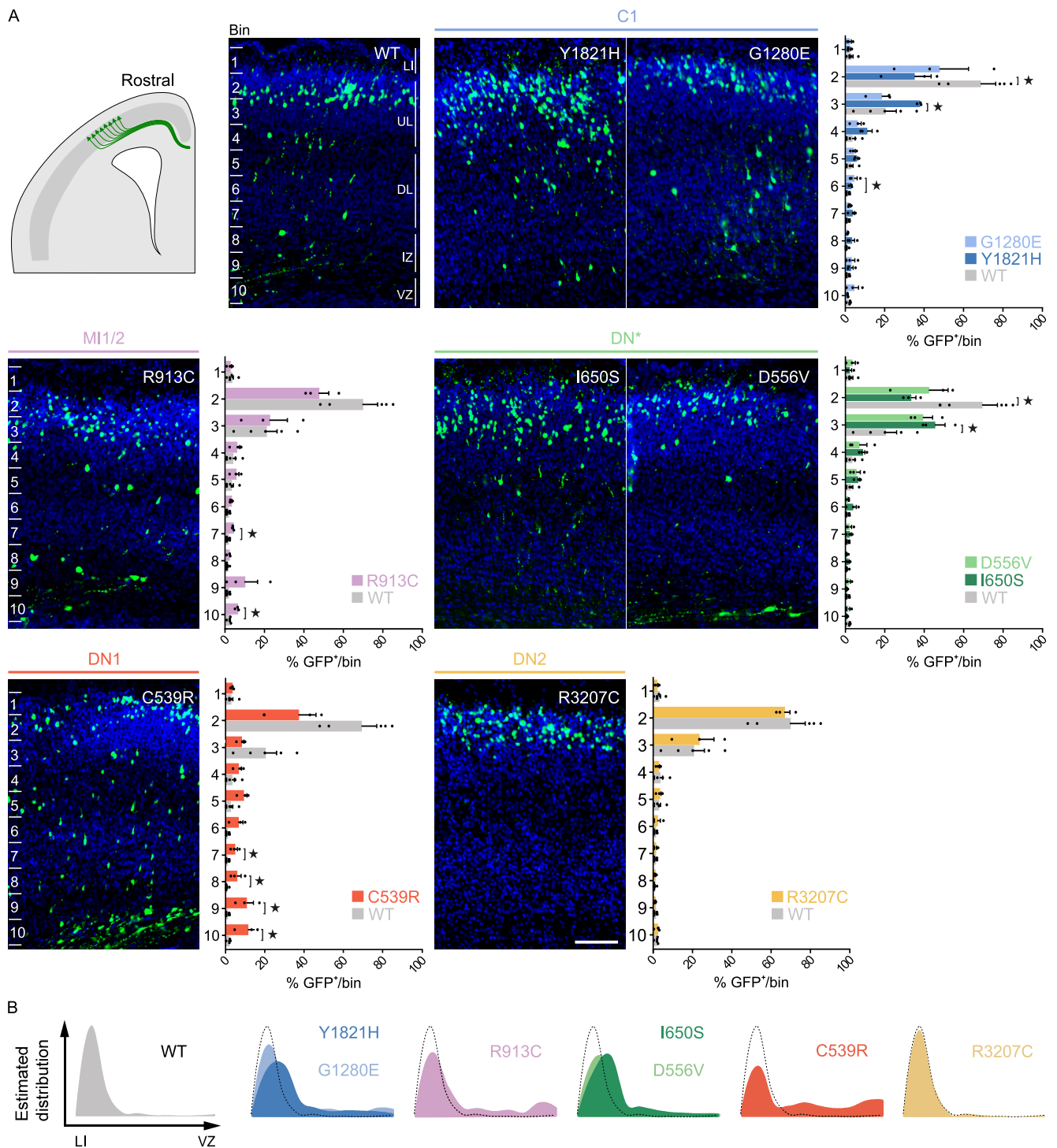
Figure 5. *RELN* **variants affect cell migration at rostral levels.** **(A)** Immunofluorescence wide-field images of P1 brains at rostral levels after IUE at E14.5. The entire thickness of the electroporated cortex was divided into 10 bins and the percentage of electroporated GFP$^+$ cells per bin was calculated (n=5 WT-RELN, n=3 mutants). Bin 1 corresponded to layer I (LI), bin 2-4 to upper layers (UL), bin 5-7 to deeper layers (DL), bin 8-9 to intermediate zone (IZ) and bin 10 to ventricular zone (VZ). Data are mean ± SEM; each symbol represents one electroporated brain; Kolmogrov-Smirnov test, ★p<0.05. Scale bar, 100 μm. **(B)** Recapitulative representation of the estimated distribution of electroporated cells from the LI to the VZ for all constructs.

Figure 6. Pachygyria-associated de novo heterozygous *RELN* variants behave as dominant-negative in vitro. (A-B) Immunoblottings (left) and densitometric analysis (right) of HEK293T cell lysates **(A)** and media **(B)** co-transfected with Y1821H and G1280E variants, or co-transfected with WT-RELN and R913C, I650S/D556V, C539R or R3207C variants, probed with anti-RELN G10 or anti-GFP antibodies. RELN signal normalized to GFP in lysates and expressed as the media (M)-to-lysate (L) ratio in the media (*n*=4-8 independent transfections). **(C-F)** Immunoblottings (left) and densitometric analysis (right) of cell lysates **(C, E)** and media **(D, F)** of HEK293T cells co-transfected with a Flag-WT-RELN and WT-RELN, R913C, I650S/D556V, C539R or R3207C variants, probed with anti-Flag, anti-RELN G10 or anti-GFP antibodies. Data is presented as described for A-B (*n*=4 independent transfections). All data are mean ± SEM; 2-tailed one sample *t* test, ★*p*<0.05, ★★*p*<0.01, ★★★*p*<0.001. (*) unspecific bands. kDa, protein standard sizes.
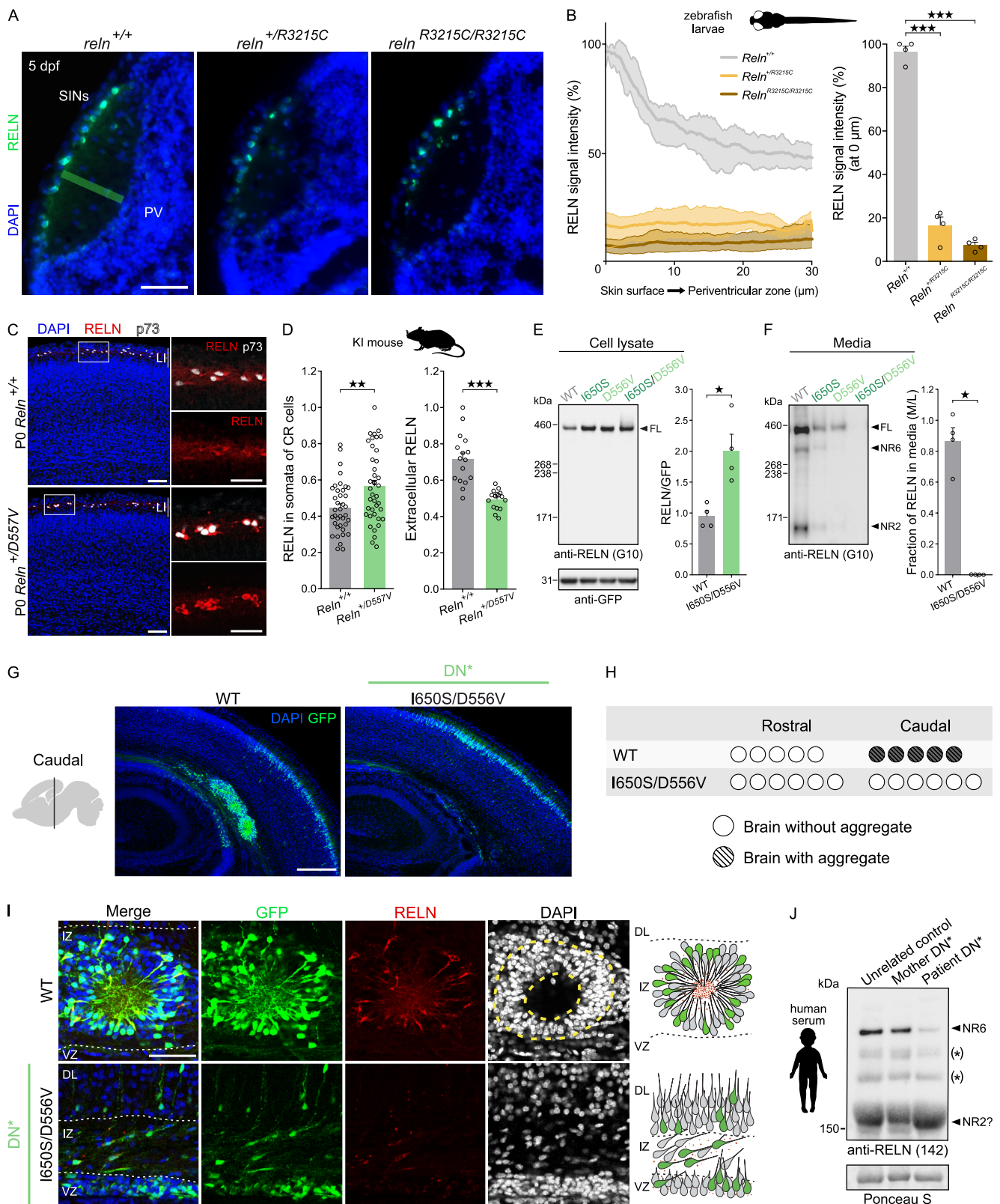
Figure 7. Pachygyria-associated de novo variants dominantly suppress RELN secretion in animal models and patients. (A) RELN (green) distribution in *Reln*^{+/+}, *Reln*[+/R3215C] and *Reln*[R3215C/R3215C] zebrafish at 5 days post-fertilization (dpf) on cryosectioned tecti, with DAPI (blue). Scale bar, 30 μm. **(B)** Densitometric plots (left) depict average RELN intensities (with minimum and maximum values) from the skin surface to the periventricular (PV) zone (green area in A) at distances 0, 10, 20 and 30 μm. SINs, superficial interneurons. Fluorescence intensities (right) at the neuropil surface. Data are mean ± SEM (n=4 animals/genotype); one-way ANOVA, Dunnett's test, ★★★p<0.001. © , Immunofluorescence images P0 *Reln*^{+/+} and *Reln*[+/D557V] neocortices with CRs expressing RELN (red) and p73 (white), with DAPI (blue). Scale bars, 75 μm. **(D)** RELN intensities in CRs somata (n=38 *Reln*^{+/+}; n=40 *Reln*[+/D557V] somata, from 4 brains/genotype) and in LI's extracellular space (n=16 ROIs, from 4 brains/genotype). Data are mean ± SEM; Welch's t test, ★★p<0.01, ★★★p<0.001. **(E-F)** Immunoblottings (left) and densitometric analysis (right) of HEK293T lysates **(E)** and media **(F)** transfected with WT-RELN or RELN-variants from DN* patient. RELN signal normalized to GFP in lysates and expressed as the media (M)-to-lysate (L) ratio in the media (n=4 independent transfections). Data are mean ± SEM; Mann-Whitney test, ★p<0.05. **(G)** Immunofluorescence images of GFP[+] (green) aggregates, with DAPI (blue), in caudal P1 mouse brains upon IUE at E14.5 of WT-RELN and I650S/D556V (n=5-6). Scale bar, 250 μm. **(H)** Analysis of aggregate formation. **(I)** Immunofluorescence images of aggregates stained for GFP (green), RELN (red) and DAPI (blue). Scale bar, 50 μm. **(J)** Representative immunoblotting (from 2 experiments) of patient DN* blood serum, healthy mother and unrelated control, with anti-RELN 142 antibodies. Ponceau S indicates equal protein loading. (*) Unspecific bands. kDa, protein standard sizes. LI, layer I; DL, deeper layers; IZ, intermediate zone, VZ, ventricular zone.